

UNCLASSIFIED

Defense Technical Information Center  
Compilation Part Notice

ADP013698

TITLE: Large-Eddy Simulation of a Subsonic Flow Over a Deep, Open Cavity

DISTRIBUTION: Approved for public release, distribution unlimited

This paper is part of the following report:

TITLE: DNS/LES Progress and Challenges. Proceedings of the Third AFOSR International Conference on DNS/LES

To order the complete compilation report, use: ADA412801

The component part is provided here to allow users access to individually authored sections of proceedings, annals, symposia, etc. However, the component should be considered within the context of the overall compilation report and not as a stand-alone technical report.

The following component part numbers comprise the compilation report:

ADP013620 thru ADP013707

UNCLASSIFIED

Best Available Copy

## LARGE-EDDY SIMULATION OF A SUBSONIC FLOW OVER A DEEP, OPEN CAVITY

L. LARCHEVÈQUE, O. LABBÉ, I. MARY AND P. SAGAUT  
ONERA

*29 av. de la division Leclerc, 92322 Châtillon cedex, France  
Tel : 33 (0)1 46 73 42 07  
email : lionel.larcheveque@onera.fr*

**Abstract.** MILES and traditional LES computations of a high subsonic flow over a deep and open cavity using wall function and 2D-3D domain coupling strategy have been carried out ( $Re_L = 6.7 \times 10^5$ ). Both Reynolds and phase averages have been computed. Results show especially good agreement with experimental data.

### 1. Introduction

High-speed flow over a cavity generates a complex flowfield whose dynamics are governed by various physical mechanisms such as shear layer instabilities, acoustic forcing, etc. This class of flows is not only of fundamental interest, but also occurs in many aerodynamic configurations, such as weapon bay or wheel wells, where large pressure fluctuations induced by this flow are known to result in possible structural damages. The capability of numerically predicting these flows in a time-accurate fashion is consequently an important issue. In the past twenty years, numerous RANS computations, mostly supersonic, have been carried out. The increase of available computational resources yet allows LES computations of such configurations.

The studied cavity has a length L to depth D ratio of 0.42, and therefore belongs to the deep cavity category. There is no reattachment of the flow on the floor (open cavity). The Reynolds number (based on the inflow velocity  $U_\infty$  and the length L of the cavity) and the Mach number are  $6.7 \times 10^5$  and 0.8 respectively. This configuration has been chosen because of the availability of an experimental data base compiled by Forestier et

al.[1], which was specially designed for the accurate evaluation of DNS and LES computations. These data include averaged and phase averaged (20 phases) velocity measurements in various locations along the channel and inside the cavity. According to this experience, the flow is characterized by a fundamental frequency of 1975 Hz. Spectrum exhibits multiple harmonics of decaying SPL levels (see left part of the figure 4). The length of a period is not constant (jitter), the standard deviation being approximatively equal to 1% of the mean value. During one period, shadowgraphs and phase averaged velocity reveal the existence of three coherent vortices (see left part of the figure 8). Shadowgraphs also show the presence of strong pressure waves.

## 2. Numerical methods

Spatial discretization is accomplished using a finite volume scheme. Two categories of computations have been carried out. The preliminary results were obtained without the use of any subgrid model, an approach known as MILES, introduced by Boris et al.[2], and which is based on the idea that an upwind scheme is able to mimic the dissipative behaviour of the small structures. According to this technique, the convective fluxes are evaluated by means of an upwinding formulation derived from the AUSM+(P) scheme originally proposed by Edwards and Liou[3]. With the intention of getting to the root of this study, a more traditional LES approach was also tested, using the mixed-scale model of Sagaut coupled with a selective function (Sagaut and Troff[4]). In that case, the second order spatial scheme is centered in order to ensure minimal numerical dissipation. To prevent the apparition of oscillations, a detector proposed by Mary[5] locally switches if necessary to the former scheme. Explicit temporal integration is achieved using a third order Runge-Kutta scheme. In order to greatly reduce the computational cost, an instantaneous log law is used at the wall. Periodic boundary conditions are set in the spanwise direction. Velocity profile is imposed at the entrance of the channel, with additional white noise velocity fluctuations. Both mean and fluctuating velocities are adjusted in concordance with experimental measurements. Non-reflective outflow boundary conditions are used on the left extremity of the channel.

The computational domain extends from -1L to 5L in the streamwise direction and from -2.4L to 2L in the vertical direction, the origin being set in the leading edge of the cavity (see figure 2 for a glimpse of the complete domain). The computation is done on a multibloc structured mesh, with 2D-3D coupling strategy. The upper side of the channel, in which the flow is almost two-dimensional, is discretized in the spanwise direction with less cells than the lower part of the channel. The remaining part of the computational domain (including the cavity) is fully 3D. Two meshes

have been employed, a coarse one with 800,000 cells and a fine one with approximatively twice this number, obtained by multiplying the number of cells in both the streamwise and normal directions by 1.5, the number of cells in the spanwise direction remaining constant. The MILES approach was tested only on the coarse mesh. The following table summarizes the typical size of the cells in wall unit for the LES computations.

Mesh	streamwise	spanwise	$\perp$ to wall
Coarse	150 - 400	50 - 200	20 - 30
Fine	100 - 300	50 - 200	15 - 20

Due to the restrictive CFL conditions, dimensionless time-steps of  $9.1 \times 10^{-4}$  on the coarse mesh and  $7.28 \times 10^{-4}$  on the fine one have been adopted.

As seen in figure 1, the procedure used to compute phase averages consists in splitting the interval between five consecutive peaks of filtered pressure into 80 sub-intervals. The goal of such an approach is to provide against dephasing due to the jitter. For all the computations the standard deviations of the length of the period were found of the same magnitude as the experimental one. Tests with experimental data have proved than with up to four by four periods splitting, the effect of the jitter is negligible. Therefore this upper value has been adopted. The averaging time for both Reynolds and phase averages corresponds to  $13 \times 4 = 52$  cavity cycles.

### 3. Numerical results and comparison with experimental data

Figures 2 and 3, based on instantaneous data issued from the fine mesh, show coherent structures highlighted using Q criterion ( $\nabla \cdot \underline{u}$  tensor  $2^{nd}$  invariant) combined with a pseudo-Schlieren view. The main characteristics of the flow are recovered, with the existence of three major structures (the two vortical tubes on the left of the figure 3 are about to pair) and pressure waves with similar shapes compared to the experimental shadowgraphs.

The experimental and computed spectra are shown in figure 4. The concordance is really good, with an accurate prediction of both the mean value and peaks levels up to 26000 Hz (12<sup>th</sup> harmonic). The frequencies of the peaks are slightly over-evaluated (2.5%), but it has to be noticed that the spectral resolution is about 2.2% of the fundamental frequency. This spectrum is obtained from fine mesh data. On the coarse mesh, the levels are decaying faster, especially with the MILES computation, and only the first four peaks are present, with the same levels as for the fine mesh.

The evolution of the incompressible momentum thickness  $\theta$  along the shear layer is plotted in figure 5. All the three computed graphs are close

of the experimental data, with the exception of an earlier effect of the trailing edge. MILES and LES computations on the coarse mesh give similar results, with a slightly underestimated growth rate in the initial region ( $5 \leq x/\theta_r \leq 20$ ). Using the fine mesh, we obtain initially a higher growth rate, but the layer grows weakly in the region  $40 \leq x/\theta_r \leq 60$ , where the flow is supposed to be near to the equilibrium. In the first region, Forestier et al.[6] suppose that the fast growth may be explained by an early pairing of small vortical tubes, a mechanism similar to the "collective interaction" introduced by Ho and Huang[7]. Therefore a plausible explanation for the higher growth rate may be that because of the refinement of the mesh, small structures in the vicinity of the leading edge and their dynamics are more accurately described.

Figures 6 shows the evolution of the vorticity thickness  $\delta$ , defined by:

$$\delta(x) = (U^+ - U^-) / \left[ \max_z \left( \frac{\partial u}{\partial z} \right) \right]$$

where  $U^+$  is the velocity in the center of the channel and  $U^-$  is the velocity inside the cavity, here considered equal to 0. Beyond  $x/\theta_r = 25$ , computations and experience are well correlated, especially when using a subgrid model. Here again, there is an earlier influence of the trailing wall. Before  $x/\theta_r = 25$ , the evaluation of the experimental values of  $\delta$  is of a poor accuracy because of the sharp vertical velocity gradient resulting from the small thickness of the shear layer and the coarse size of the measure mesh.

Figure 7 presents Reynolds and phase averaged streamwise velocity and 2D turbulent kinetic energy profiles at a location corresponding to  $x/\theta_r = 50$ , in the middle of the self-similarity growth region. Focusing on the streamwise velocity, we see that the LES profiles associated with the coarse and the fine meshes are almost indistinguishable. MILES profiles differ mainly inside the cavity, with smaller speed. However for each case the agreement with experimental data is good. If we consider the turbulent kinetic energy profiles, the two types of LES calculations are still closely connected. On Reynolds average, MILES computation generates more turbulent kinetic energy. On the contrary, LES leads to slightly underestimated turbulent kinetic energy peaks, but the shapes are correct. The two phases selected show deficit in energy for each case, when the locations of the peaks are well predicted.

Figure 8 shows a comparison of the loci of the coherent structures between experimental data and numerical results on the fine mesh, for four different phases. The structures are highlighted using the Weiss criterion (equivalent to 2D Q criterion). If we consider that the experimental measurement mesh is really coarse compared with the computing mesh and that this difference between the two meshes has an important effect on the computation of  $\nabla \underline{u}$ , it stands to reason that the overall agreement is excellent.

Each experimental structure can be linked to a numerical structure with quite correct location and size, except perhaps for the less energetic ones (see structure 3 in phase 11). The results of the computation on the coarse mesh (MILES and LES), which are not shown here, are closely similar to the results on the fine mesh. As a remark, we can notice that the figures 2 and 3 correspond to a time which takes place into the first phase.

#### 4. Conclusion

All the computations presented here show good agreement with the experimental data. This similarity despite various numerical methods and meshes may be explained by the energetic predominance of the low frequencies (and therefore the large structures). These simulations have then proved the (MI)LES techniques capability of studying this category of cavity problems, and therefore the possibility to use them to improve our understanding of the flow dynamics inside and above the cavity.

#### References

1. N. Forestier, P. Geffroy, and L. Jacquin. Flow over cavities in transonic regime: a test case for numerical simulations. In *Proceedings of the First International Symposium on Turbulence Shear Flow Phenomena*, pages 933-938, September 11-15, 1999.
2. J. P. Boris, F. F. Grinstein, E. S. Oran, and R. L. Kolbe. New insights into large-eddy simulation. *Fluid Dyn. Res.*, 10:199-228, 1992.
3. J.R. Edwards and M.S. Liou. Low-diffusion flux-splitting methods for flows at all speed. *AIAA Journal*, 36:1610-1617, 1998.
4. P. Sagaut and B. Troff. Subgrid-scale improvement for non-homogeneous flows. In *First AFOSR International Conference on DNS and LES*, Ruston, USA, August 4-8, 1997.
5. I. Mary and P. Sagaut. LES of a flow around an airfoil near stall. *AIAA paper*, 2001-2559, 2001.
6. N. Forestier, L. Jacquin, and P. Geffroy. The flow-field over a deep cavity at high-subsonic speed. Submitted to *J. Fluid Mech.*
7. C.-M. Ho and L.-S. Huang. Subharmonics and vortex merging in mixing layers. *J. Fluid Mech.*, 119:443-473, 1982.

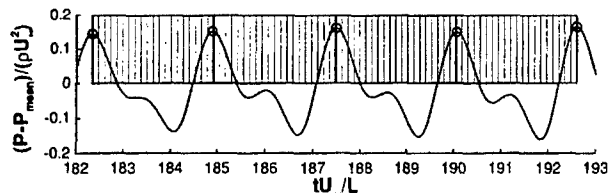


*Figure 1.* Procedure to compute phase averages : localization of maxima  $P_{max}$  for filtered pressure fluctuations and splitting of the interval between  $P_{max}^i$  and  $P_{max}^{i+4}$  into 80 sub-intervals with equal duration.

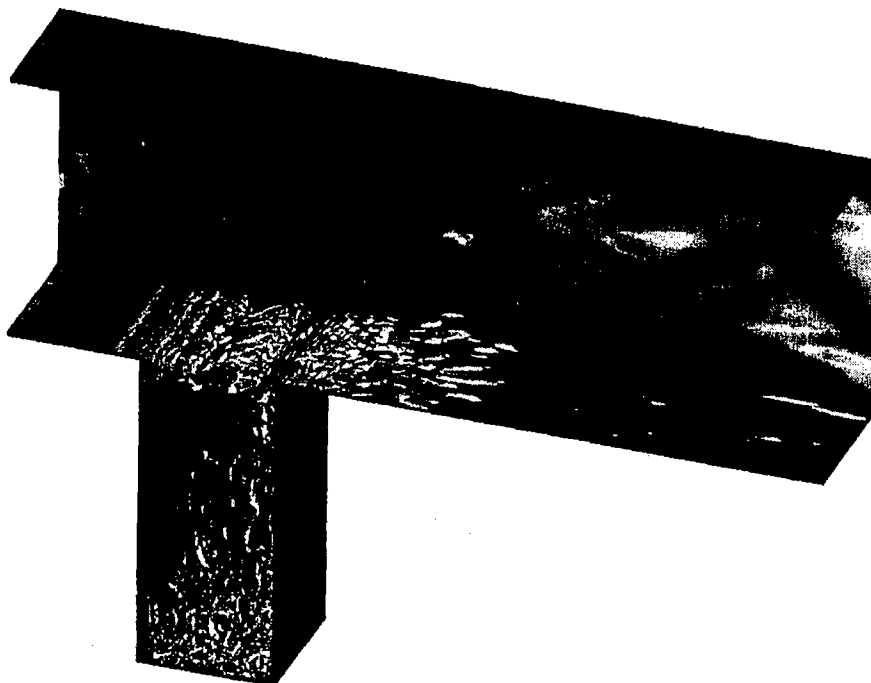


Figure 2. View of the computational domain. Structures are visualized using iso-surface of  $Q$  equal to  $10 \left(\frac{U_\infty}{L}\right)^2$  combined with a Schlieren-like picture in the background.



Figure 3. Closeup view of the mixing layer above the cavity:  $Q$  value equal to  $20 \left(\frac{U_\infty}{L}\right)^2$ .

---

# Best Available Copy

LES OF A SUBSONIC FLOW OVER A CAVITY

765

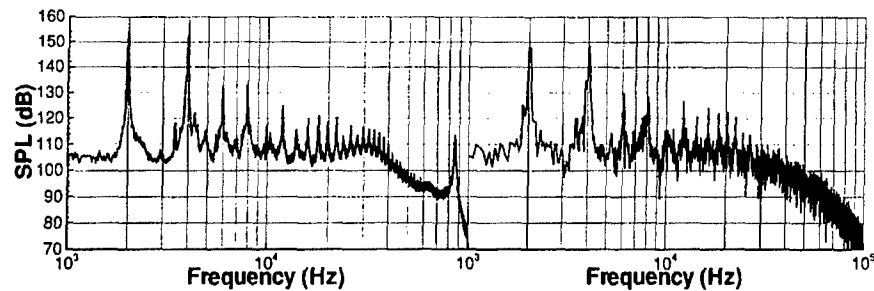


Figure 4. Experimental (left) and computed (right) spectra. The computation is done on the fine mesh with subgrid model (LES).

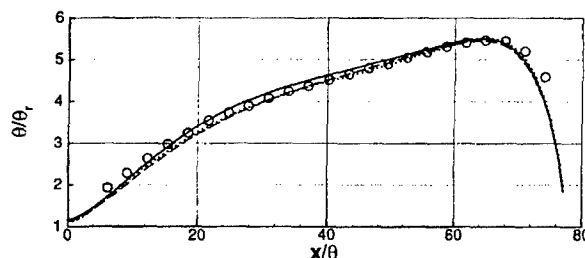


Figure 5. Momentum thickness  $\theta$  of the mixing layer normalized with initial experimental momentum thickness  $\theta_r$ . .....: MILES with coarse mesh; - - -: LES with coarse mesh; ——: LES with fine mesh; o: experimental data.

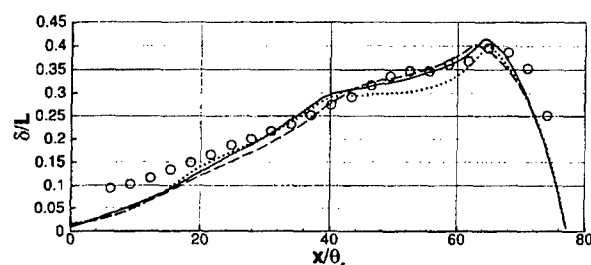


Figure 6. Vorticity thickness  $\delta$  of the mixing layer normalized with  $L$ . .....: MILES with coarse mesh; - - -: LES with coarse mesh; ——: LES with fine mesh; o: experimental data.

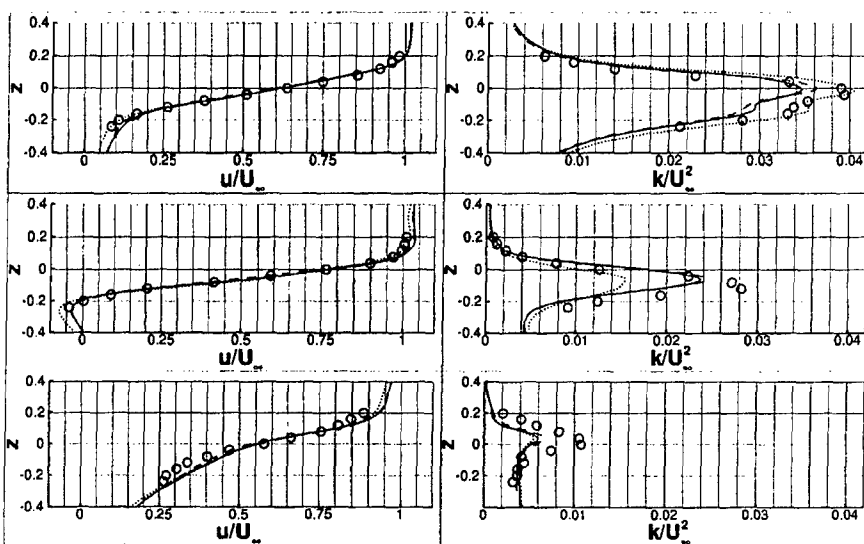


Figure 7. Mean streamwise velocity (left) and 2D turbulent kinetic energy (right) profiles at  $x = 0.6L$ : Reynolds average (top), phase average for phase 1 (middle) and phase average for phase 11 (bottom). . . . .: MILES on coarse mesh; - - -: LES on coarse mesh; ——: LES on fine mesh; o: experimental data.

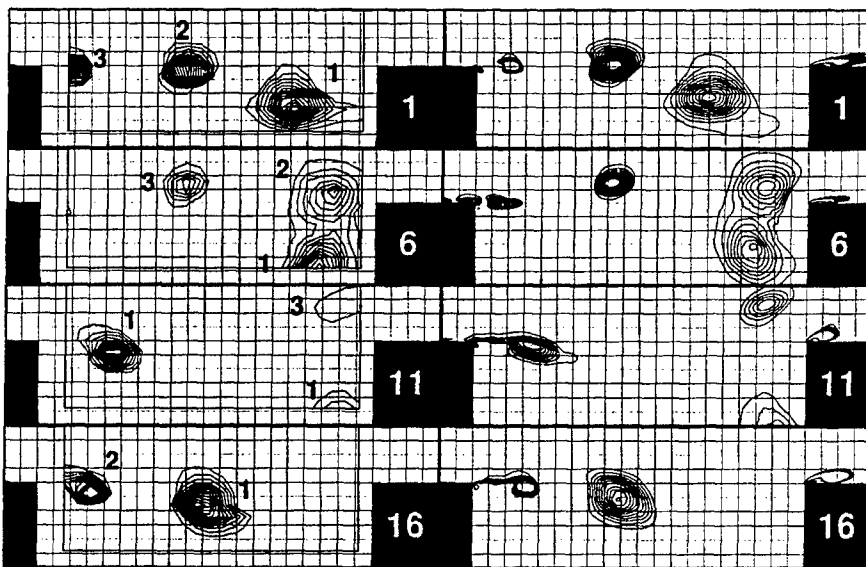


Figure 8. Phase averaged coherent structures isolated using Weiss criterion (levels from 1 to 25 by increment steps of 2, normalized using  $(\frac{U_\infty}{L})^2$ ): experimental data (left) and LES on fine mesh (right) for phases 1, 6, 11 and 16.